Streak breakdown instability in pipe Poiseuille flow

Álvaro Meseguer[a)]
Oxford University Computing Laboratory, Wolfson Building, Parks Road, Oxford OX1 3QD, United Kingdom

(Received 12 July 2002; accepted 23 January 2003; published 2 April 2003)

This work is devoted to the study of the stability of Hagen–Poiseuille flow or pipe flow. The analysis is focused on the *streak breakdown* process by which two-dimensional streamwise-independent finite amplitude perturbations transiently modulate the basic flow leading to a profile that contains saddle points and is linearly unstable with respect to very small streamwise-dependent perturbations. This mechanism is one possible route of transition to turbulence in subcritical shear flows. The exploration is carried out for initial disturbances of different finite amplitudes and axial and azimuthal periodicity. This study covers a wide range of Reynolds numbers and the double threshold curve obtained for transition is consistent with experimental observations. © *2003 American Institute of Physics.* [DOI: 10.1063/1.1564093]

I. INTRODUCTION

Hydrodynamic instability of pipe flow remains one of the oldest and yet unsolved problems of fundamental fluid dynamics. Pipe or plane Couette problems belong to a particular family of shear flows which are usually termed *subcritical*.[1] From a mathematical point of view, these flows are linearly stable, i.e., the spectrum of the linearized Navier–Stokes operator around the basic flow always lies on the stable half of the complex plane. Therefore, any infinitesimal perturbation added to the basic flow must eventually decay. Nevertheless, these flows become turbulent in the laboratory. For instance, below a critical Reynolds number, Re_c, in the range $1760 \lesssim \mathrm{Re}_c \lesssim 2300$, pipe Poiseuille flow does not exhibit a sustained transition to turbulence.[2,3] For Reynolds numbers higher than Re_c, a finite amplitude disturbance is required to destabilize the flow. Experimental and numerical evidence suggest that transition in pipe flow is extremely sensitive to the size and structure of the perturbations. Pipe flow instability differs from that of other classical flows such as Taylor–Couette or Rayleigh–Benard where the basic profile becomes unstable by means of a local bifurcation.[1] In those problems, the instability is characterized by a sharp critical value of the control parameter, the Reynolds number or the Rayleigh number, above which the basic flow becomes linearly unstable. In that case, the agreement between experimental results and numerical simulations is very good. Besides, in these problems, the flow is confined to a finite size domain, i.e., they are *enclosed* flows. Pipe flow is a prototype of *open* flow and its study is more complicated. In open flows, the perturbations are eventually advected downstream and they leave the domain, making it impossible sometimes to determine the laminar-turbulent character of the dynamics for long times. Another difficulty arises when the open flows are modelled numerically by artificially assuming periodicity in the streamwise direction of the flow.

The numerical simulation of pipe flows is not a new matter. This problem has been previously simulated by different numerical schemes in the past.[4–9] In recent works,[10,11] the linear stability and transient growth of perturbations in pipe flow were studied by means of the linearization of the Navier–Stokes equations and it was found that streamwise-independent vortices were optimally amplified by linear nonnormal mechanisms. It has long been known that streamwise vortices and nonnormality of the linear operator are two crucial requirements for the subcritical transition to turbulence in shear flows.[12,13] These two-dimensional structures grow transiently and modulate the basic flow, leading to a new velocity profile which contains *streaks*, i.e., regions where the flow attains high or low relative axial speeds. This new flow contains saddle points and, in a transient sense, is linearly unstable with respect to three-dimensional perturbations.[14]

In a beautiful work, Zikanov[15] analyzed the stability of the Hagen–Poiseuille flow by means of adding streamwise-independent finite amplitude perturbations to the basic flow and exploring the linear stability of the resulting time-dependent streaks with respect to infinitesimal streamwise-dependent disturbances. Zikanov concluded that this time-dependent flow was linearly unstable with respect to certain streamwise-dependent perturbations with a preferred axial periodicity, depending on the Reynolds number and the initial amplitude of the two-dimensional perturbation. This suggests that the streaks would eventually be destabilized leading to the usually termed *streak breakdown* scenario. Therefore, the main goal of this work will be to study the nonlinear time evolution of a particular type of perturbations in pipe flow and to identify the streak breakdown mechanism as a possible route to turbulence in this particular problem. We will focus our attention on the early stages of transition

[a)]Present address: Department de Fisica Aplicada, Univ. Politècnica de Catalunya, C/Jordi Girona 1-3, Mod. B5, 08034 Barcelona, Spain; electronic mail: alvar@fa.upc.es

to turbulence; the study of fully developed turbulent flow is beyond our scope.

The paper is structured as follows. In Sec. II we formulate the problem mathematically and the numerical methods used are outlined. Section III is devoted to the study of the formation streaks, as a result of introducing streamwise-independent perturbations. In Sec. IV we provide a comprehensive exploration of the streak nonlinear instability by adding a very small streamwise-dependent component in the perturbation field. This section leads to the exploration carried out in Sec. V, where we determine the critical amplitude of transition for a wide range of Reynolds numbers. Finally, we have included an Appendix devoted to the spectral formulation of the numerical method.

II. MATHEMATICAL FORMULATION AND NUMERICAL METHODS

We consider the motion of an incompressible viscous fluid of kinematic viscosity ν and density ρ. The fluid is driven through a circular pipe of radius a and infinite length by a uniform pressure gradient, Π_0, parallel to the axis of the pipe. The motion of the fluid is governed by the incompressible Navier–Stokes equations

$$\partial_t \mathbf{v} + (\mathbf{v}\cdot\boldsymbol{\nabla})\mathbf{v} = -\frac{\Pi_0}{\rho}\hat{\mathbf{z}} - \nabla p + \nu\Delta\mathbf{v}, \tag{1}$$

$$\boldsymbol{\nabla}\cdot\mathbf{v} = 0, \tag{2}$$

where $\mathbf{v}$ is the velocity vector field, satisfying the no-slip boundary condition at the wall,

$$\mathbf{v}_{\text{pipe wall}} = \mathbf{0}, \tag{3}$$

and p is the reduced pressure. We formulate the problem in cylindrical coordinates. The velocity of the fluid is prescribed by its radial ($\hat{\mathbf{r}}$), azimuthal ($\hat{\boldsymbol{\theta}}$), and axial ($\hat{\mathbf{z}}$) components

$$\mathbf{v} = u\hat{\mathbf{r}} + v\hat{\boldsymbol{\theta}} + w\hat{\mathbf{z}} = (u,v,w), \tag{4}$$

where u, v, and w depend on the three spatial coordinates (r,θ,z) and time t. A basic steady solution of Eqs. (1), (2), and (3) is the so-called *Hagen–Poiseuille flow*

$$\mathbf{v}_B = (u_B, v_B, w_B) = \left(0,0,-\frac{\Pi_0 a^2}{4\rho\nu}\left[1-\left(\frac{r}{a}\right)^2\right]\right),$$
$$p_B = \Pi_0 z + C, \tag{5}$$

where C is an arbitrary constant. This basic flow is a parabolic axial velocity profile which only depends on the radial coordinate.[16] The velocity of the fluid attains a maximum value $U_{CL} = -\Pi_0 a^2/4\rho\nu$ at the center-line or axis of the cylinder.

Henceforth, all variables will be rendered dimensionless using a and U_{CL} as space and velocity units, respectively. The axial coordinate z is unbounded since the length of the pipe is infinite. In what follows, we assume that the flow is axially periodic with period b. This assumption, though physically artificial, enables us to study many phenomena for an infinite pipe provided b is not too small. In the dimensionless system, the spatial domain Ω of the problem is

$$\Omega = \{(r,\theta,z) \,|\, 0 \leqslant r \leqslant 1, \quad 0 \leqslant \theta < 2\pi, \quad 0 \leqslant z < Q\}, \tag{6}$$

where $Q = b/a$. In the new variables, the basic flow takes the form

$$\mathbf{v}_B = (u_B, v_B, w_B) = (0,0,1-r^2). \tag{7}$$

Finally, the parameter which governs the dynamics of the problem is the *Reynolds number*

$$\mathrm{Re} = \frac{aU_{CL}}{\nu}. \tag{8}$$

For the stability analysis, we suppose that the basic flow is perturbed by a solenoidal velocity field vanishing at the pipe wall

$$\mathbf{v}(r,\theta,z,t) = \mathbf{v}_B(r) + \mathbf{u}(r,\theta,z,t), \quad \boldsymbol{\nabla}\cdot\mathbf{u} = 0, \quad \mathbf{u}(r=1) = \mathbf{0}, \tag{9}$$

and a perturbation pressure field

$$p(r,\theta,z,t) = p_B(z) + q(r,\theta,z,t). \tag{10}$$

On introducing the perturbed fields in the Navier–Stokes equations, we obtain a nonlinear initial-boundary problem for the perturbations $\mathbf{u}$ and q:

$$\partial_t \mathbf{u} = -\nabla q + \frac{1}{\mathrm{Re}}\Delta\mathbf{u} - (\mathbf{v}_B\cdot\boldsymbol{\nabla})\mathbf{u} - (\mathbf{u}\cdot\boldsymbol{\nabla})\mathbf{v}_B - (\mathbf{u}\cdot\boldsymbol{\nabla})\mathbf{u}, \tag{11}$$

$$\boldsymbol{\nabla}\cdot\mathbf{u} = 0, \tag{12}$$

$$\mathbf{u}(1,\theta,z,t) = 0, \tag{13}$$

$$\mathbf{u}(r,\theta+2\pi n,z,t) = \mathbf{u}(r,\theta,z,t), \tag{14}$$

$$\mathbf{u}(r,\theta,z+lQ,t) = \mathbf{u}(r,\theta,z,t), \tag{15}$$

$$\mathbf{u}(r,\theta,z,0) = \mathbf{u}_0, \quad \boldsymbol{\nabla}\cdot\mathbf{u}_0 = 0, \tag{16}$$

for $(n,l) \in \mathbb{Z}^2$, $(r,\theta,z) \in [0,1]\times[0,2\pi)\times[0,Q)$ and $t > 0$. Equation (11) describes the nonlinear space-time evolution of the perturbation of the velocity field. Equation (12) is the solenoidal condition for the perturbation, and Eqs. (13)–(15) describe the homogeneous boundary condition for the radial coordinate and the periodic boundary conditions for the azimuthal and axial coordinates respectively. Finally, Eq. (16) is the initial solenoidal condition for the perturbation field at $t = 0$.

We discretize the perturbation field $\mathbf{u}$ in Eqs. (11)–(16) by a spectral approximation $\mathbf{u}_S$ of order L in z, order N in θ, and order M in r,

$$\mathbf{u}_S(r,\theta,z,t) = (u_S, v_S, w_S) = \sum_{l=-L}^{L}\sum_{n=-N}^{N}\sum_{m=0}^{M} a_{lnm}(t)\boldsymbol{\Phi}_{lnm}(r,\theta,z), \tag{17}$$

where $\boldsymbol{\Phi}_{lnm}$ are *trial* bases of solenoidal vector fields of the form

$$\boldsymbol{\Phi}_{lnm}(r,\theta,z) = e^{i(2\pi lz/Q + n\theta)}\mathbf{v}_{lnm}(r), \tag{18}$$

satisfying

$$\boldsymbol{\nabla}\cdot\boldsymbol{\Phi}_{lnm} = 0, \tag{19}$$

for $l=-L,\ldots,L$, $n=-N,\ldots,N$ and $m=0,...,M$.[11] The trial bases (18) are analytic, periodic in the axial and azimuthal directions, and satisfy homogeneous boundary conditions,

$$\mathbf{\Phi}_{lnm}(1,\theta,z)=\mathbf{0}, \tag{20}$$

at the wall. Therefore, Eqs. (12)–(15) are identically satisfied by our spectral approximation. The spectral Petrov–Galerkin scheme is accomplished by substituting expansion (17) in Eq. (11) and projecting over a set of *test* vector fields

$$\mathbf{\Psi}_{lnm}(r,\theta,z)=e^{i(2\pi lz/Q+n\theta)}\tilde{\mathbf{v}}_{lnm}(r), \tag{21}$$

satisfying

$$\boldsymbol{\nabla}\cdot\mathbf{\Psi}_{lnm}=0. \tag{22}$$

Explicit expressions for the trial and test fields, $\mathbf{v}_{lnm}$ and $\tilde{\mathbf{v}}_{lnm}$, can be found in the Appendix. Overall, the projection scheme is summarized by

$$(\mathbf{\Psi}_{lnm},\partial_t\mathbf{u}_S)=\left(\mathbf{\Psi}_{lnm},\frac{1}{\mathrm{Re}}\boldsymbol{\Delta}\mathbf{u}_S-(\mathbf{v}_B\cdot\boldsymbol{\nabla})\mathbf{u}_S-(\mathbf{u}_S\cdot\boldsymbol{\nabla})\mathbf{v}_B-(\mathbf{u}_S\cdot\boldsymbol{\nabla})\mathbf{u}_S\right), \tag{23}$$

for $l=-L,\ldots,L$, $n=-N,\ldots,N$ and $m=0,...,M$, where the inner product $(\cdot,\cdot)$ is the volume integral over the domain of the pipe:

$$(\mathbf{a},\mathbf{b})=\int_0^Q\int_0^{2\pi}\int_0^1\mathbf{a}^*\cdot\mathbf{b}r\,dr\,d\theta\,dz. \tag{24}$$

We have not included the pressure term ∇q of Eq. (11) in the projection scheme (23). One of the advantages this method is that the pressure term is cancelled in the projection, i.e.,

$$(\mathbf{\Psi}_{lnm},\nabla q)=0; \tag{25}$$

see Canuto *et al.*[17] or Leonard and Wray,[18] for example.

Once the projection has been carried out, the spatial dependence has been eliminated from the problem and a nonlinear dynamical system for the amplitudes a_{lnm} is obtained. Symbolically, this system reads

$$\mathbb{A}^{lnm}_{pqr}\dot{a}_{pqr}=\mathbb{B}^{lnm}_{pqr}a_{pqr}-b_{lnm}(a,a), \tag{26}$$

where we have used the convention of summation with respect to repeated indices. The discretized operators $\mathbb{A}$ and $\mathbb{B}$ appearing in Eq. (26) are the projections

$$\mathbb{A}^{lnm}_{pqr}=(\mathbf{\Psi}_{lnm},\mathbf{\Phi}_{pqr}) \tag{27}$$

and

$$\mathbb{B}^{lnm}_{pqr}=\left(\mathbf{\Psi}_{lnm},\frac{1}{\mathrm{Re}}\boldsymbol{\Delta}\mathbf{\Phi}_{pqr}-(\mathbf{v}_B\cdot\boldsymbol{\nabla})\mathbf{\Phi}_{pqr}-(\mathbf{\Phi}_{pqr}\cdot\boldsymbol{\nabla})\mathbf{v}_B\right). \tag{28}$$

The quadratic form $b_{lnm}(a,a)$ appearing in Eq. (26) corresponds to the projection of the nonlinear convective term

$$b_{lnm}=(\mathbf{\Psi}_{lnm},(\mathbf{u}_S\cdot\boldsymbol{\nabla})\mathbf{u}_S). \tag{29}$$

For computational efficiency, this term has to be calculated via a de-aliased pseudospectral method.[17] Finally, the initial value problem is prescribed by the coefficients a^0_{lnm} representing the initial vector field $\mathbf{u}^0_S$ given by

$$a^0_{lnm}=a_{lnm}(t=0)=(\mathbf{\Psi}_{lnm},\mathbf{u}^0_S). \tag{30}$$

For the time integration of Eq. (26) we have used a fourth-order implicit backwards differentiation method for the linear terms in combination with a fourth order explicit Adams–Bashforth method[19] for the nonlinear ones. The time marching process was started with a fully explicit fourth-order Runge–Kutta algorithm.[20]

III. STREAMWISE STREAKS

In this section, we study the nonlinear evolution of streamwise independent perturbations, henceforth referred as 2D-perturbations, recently studied by Zikanov.[15] From the equation of the perturbation (11) it is straightforward to see that an initial streamwise-independent field remains independent of z for all time $t>0$, i.e., the nonlinear terms preserve their streamwise symmetry provided that the basic flow has axial component only. Zikanov exploited this property to split the perturbation as a sum of finite amplitude 2D-perturbations and infinitesimal streamwise-dependent 3D-perturbations.

We define the *energy* of an arbitrary vector field $\mathbf{u}$ as the inner product

$$E(\mathbf{u})=\frac{1}{2}\int_0^Q dz\int_0^{2\pi}d\theta\int_0^1 r\,dr\mathbf{u}^*\cdot\mathbf{u}. \tag{31}$$

With the previous definition, a straightforward calculation leads to the energy of the Hagen–Poiseuille flow,

$$E_{HP}=\frac{\pi}{6}Q. \tag{32}$$

Henceforth, we will normalize the energy of the perturbations with respect to the basic quantity E_{HP}. We define the *relative energy*, or more briefly just ''energy,'' of an arbitrary perturbation $\mathbf{u}$ as the ratio

$$\epsilon(\mathbf{u})=\frac{E(\mathbf{u})}{E_{HP}}. \tag{33}$$

For the comparison with the computations carried out by Zikanov we consider a perturbation of energy ϵ_0 with initial condition $\mathbf{u}^0_S$ in Eq. (30), which is prescribed by field

$$\mathbf{u}^0_{2\mathrm{D}}=A_0\mathbf{\Phi}^{(1)}_{010}+\mathrm{c.c.}, \tag{34}$$

where $\mathbf{\Phi}^{(1)}_{010}$ is given by Eq. (A4) and A_0 is a real constant such that $\epsilon(\mathbf{u}^0_S)=\epsilon_0$. This is equivalent to considering the simplest analytic nonaxisymmetric streamwise-independent field, with azimuthal wave number $n=1$. As a result, the initial perturbation has radial and azimuthal velocity components, the axial one being zero. We have computed the evolution of the initial condition (34) for different initial energies. For this particular computation, we have used $M=6$ radial solenoidal modes and $N=9$ azimuthal with $\Delta t=0.1$. In Fig. 1 we have plotted the $G(t)$ growth factor of the perturbation, defined as

$$G(t)=\frac{\epsilon(t)}{\epsilon_0}, \tag{35}$$

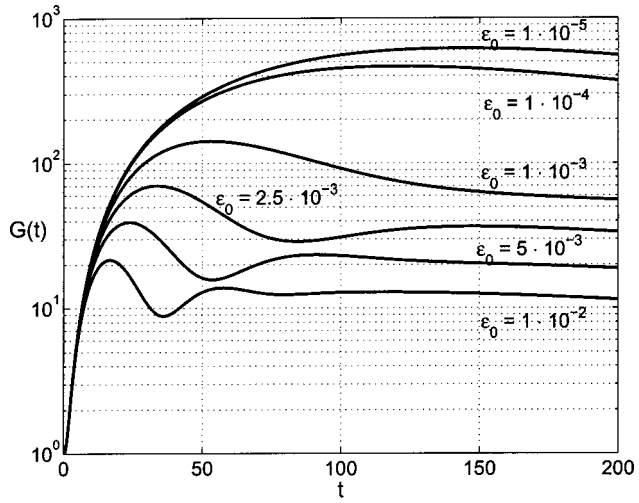

FIG. 1. Growth factor $G(t)$ for different initial energies for Re=3000. This plot was generated using $N=9$ azimuthal modes, $M=6$ radial modes and $\Delta t=0.1$, but further experiments show that it is converged to plotting accuracy.

originally considered by other authors[4,10] in the transient growth analysis of pipe flow.

In all cases studied, the agreement with Zikanov's computations is very good. As long as the initial energy goes to zero, the nonlinear effects become negligible and the dynamics is governed by the linear nonnormal mechanism. This is clearly seen in the top curve (for $\epsilon_0=1\times10^{-5}$), where the amplification factor reaches a maximum value of $G\sim620$ for $t\sim143$. This is in agreement with the former linear analyses,[10,11] where the maximum amplification factor was $G_{\max}\sim649$ for $t\sim147$. In Fig. 2 we have plotted the modulated axial flow, w_B+w_S, at $t=0$, $t=17$, $t=75$ and $t=150$, corresponding to the curve $\epsilon_0=1\times10^{-2}$ of Fig. 1 and Re=3000. In Schmid and Henningson,[10] for example, the maximum transient growth was obtained via the singular value decomposition of the exponential map of the linearized Navier–Stokes operator. This procedure gives the optimal initial conditions as right singular vectors that optimize the growth for a prescribed time. In our computations, we have considered the simplest initial streamwise vortex reproducible by our Galerkin approximation, providing 96% of the optimal growth computed with nonmodal linear methods. Figure 2(d) recovers the computation originally carried out by Zikanov for the same initial energy. For $t=150$, we can observe the formation of streaks by the lift-up effect, where high speed axial flow is driven to low axial speed regions near the wall.[21] The first important feature of this transient flow is the presence of saddle points in its profile. This would lead to an inviscid instability when perturbing the flow with 3D-disturbances. The second is that this transient regime is almost steady, as we observe more clearly from the bottom curve in Fig. 1, where the amplitude of the perturbation is almost constant for a long period of time. This feature provides the flow the property of being potentially unstable when 3D-infinitesimal perturbations are present, provided

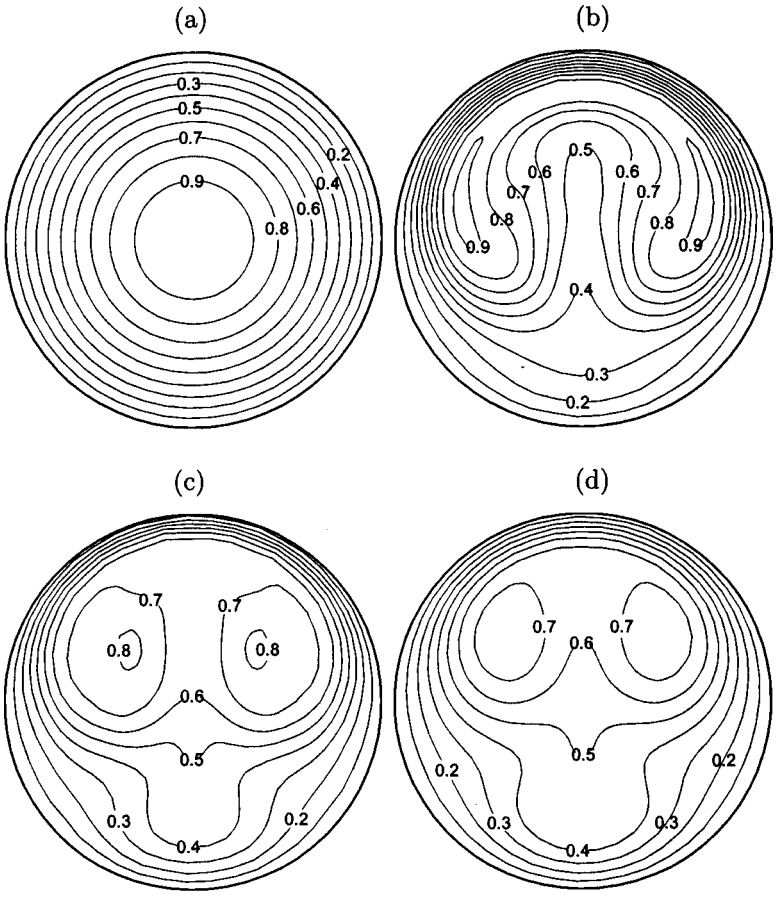

FIG. 2. Formation of streaks for the Re=3000 and $\epsilon_0=1\times10^{-2}$. Modulated axial flow w_B+w_S at: (a) $t=0$; (b) $t=17$; (c) $t=75$; and (d) $t=150$.

that the formation of streaks occurs before the viscous effects become significant. This stability analysis can be carried out by linearizing the Navier–Stokes equations in a neighborhood of the quasi-steady modulated 2D-flow. This is Zikanov's approach; he studied the linear evolution of three-dimensional perturbations once the streaks were already developed. Zikanov observed transient exponential growth of 3D-perturbations for some range of axial wave numbers as a clear indication that the 2D-streaks, even quasi-steady, are linearly unstable.

IV. STREAK BREAKDOWN

In this section we study the nonlinear evolution of very small 3D-perturbations superimposed to the 2D-initial disturbances considered in the previous section. According to the explorations provided by Zikanov, there are three factors that determine the efficiency of the streak instability. The first factor is the initial amplitude of the 2D-perturbation. The second one is the fundamental axial wave number, $k=2\pi/Q$, of the 3D-perturbation. The efficiency of the exponential instability of the streaks strongly depends on the combination of the last two factors. For a given amplitude of the initial 2D-perturbation, there is always an optimal axial wave number which exhibits a maximum growth. This axial wave number goes to zero as long as the initial amplitude decreases, as expected from the nonmodal analysis carried out by Schmid and Henningson.[10] Finally, the efficiency of the instability mechanism is strengthened when increasing the Reynolds number, the third factor. Another aspect that should be considered would probably be the time at which the 3D-perturbations are added to the modulated 2D-flow. For example, Zikanov fixed this time to $t=30$ for all his computations, provided that the streaks were already developed at that time in the particular cases he studied.

Our exploration differs from Zikanov's analysis in three different aspects. First, we solve the full nonlinear Navier–Stokes problem so the 3D-perturbations evolve dictated not only by the linear advective coupling with the basic flow and the 2D-streaks but also by the three-dimensional nonlinearities. Second, we include the 3D-perturbations from the beginning rather than including them once the streaks are developed. The reason for doing this is that we do not know *a priori* what time will the streaks require to appear since the initial amplitude of the perturbation and the Reynolds number will be different for each one of our explorations. Third, we fix a particular axial wave number of the 3D-perturbations based on Zikanov's explorations; a comprehensive study for different axial periodicities is computationally very expensive. More specifically, we have considered those axial modes that provided an optimal growth in the time-dependent linear analysis.

In what follows, we split the initial perturbation in two parts

$$\mathbf{u}_S^0=\mathbf{u}_{2D}^0+\mathbf{u}_{3D}^0, \tag{36}$$

where $\mathbf{u}_{2D}^0$ is the streamwise-independent component given by

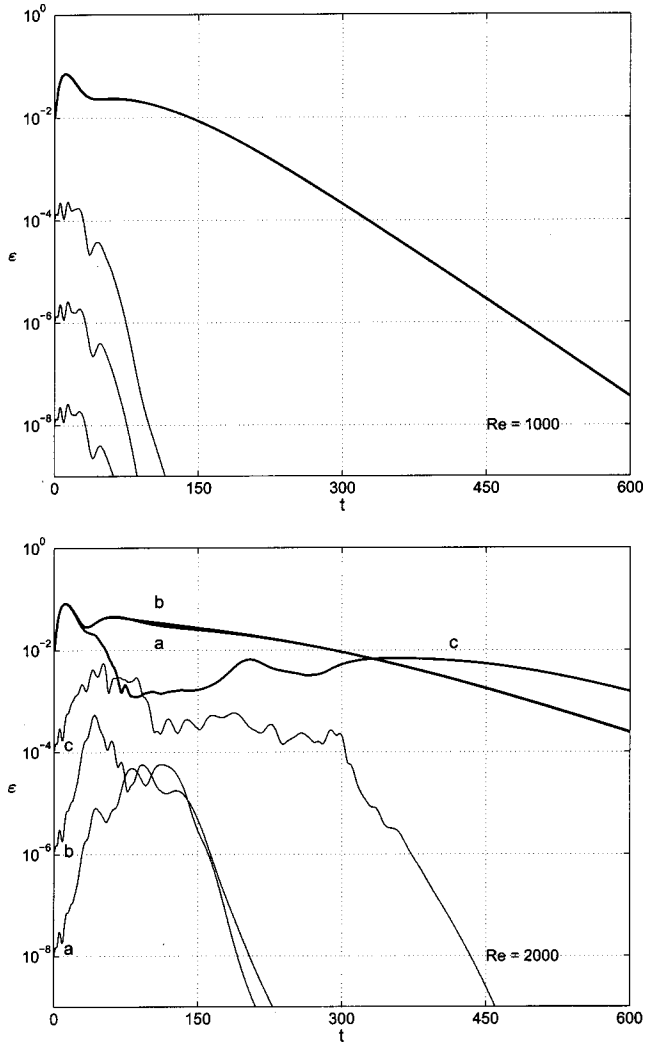

FIG. 3. Time evolution of the energy of 2D (thick curves) and 3D (thin curves) perturbations for different values of Re. For these computations, the aspect ratio was $Q=\pi$ (i.e., the lowest nonzero axial wave number is $k=2$). We used $M=14$ modes in r, $N=7$ in θ and $L=1$ in z. The time step is $\Delta t=5\times10^{-2}$. In each one of the cases, we have not found any qualitative difference when increasing the spectral order. For legends, see text.

$$\mathbf{u}_{2D}^0=A_0\boldsymbol{\Phi}_{010}^{(1)}+\text{c.c.}, \tag{37}$$

and $\mathbf{u}_{3D}^0$ is the streamwise-dependent contribution,

$$\mathbf{u}_{3D}^0=A_1(\boldsymbol{\Phi}_{110}^{(1)}+\boldsymbol{\Phi}_{100}^{(1)})+\text{c.c.}, \tag{38}$$

where $\boldsymbol{\Phi}_{010}^{(1)}$, $\boldsymbol{\Phi}_{110}^{(1)}$, and $\boldsymbol{\Phi}_{100}^{(1)}$ are given in the Appendix and the factors A_0 and A_1 are suitable constants so that the energy of the 2D and 3D modes is distributed as follows:

$$\boldsymbol{\epsilon}(\mathbf{u}_{2D}^0)=\boldsymbol{\epsilon}_0^{2D}, \quad \boldsymbol{\epsilon}(\mathbf{u}_{3D}^0)=\boldsymbol{\epsilon}_0^{3D}, \tag{39}$$

for prescribed values $\boldsymbol{\epsilon}_0^{2D}$ and $\boldsymbol{\epsilon}_0^{3D}$, satisfying $\boldsymbol{\epsilon}_0^{3D}\ll\boldsymbol{\epsilon}_0^{2D}$.

In Figs. 3 and 4, we have plotted the time evolution of the energies $\boldsymbol{\epsilon}^{2D}(t)$ and $\boldsymbol{\epsilon}^{3D}(t)$, corresponding to the 2D and 3D perturbations, respectively. The computations have been made for Reynolds numbers increasing from Re=1000 to Re=3000 and for $Q=\pi$; i.e., the lowest nonzero axial wave number is $k=2$. We have selected this axial periodicity according to the computations carried out by Zikanov, where the optimal wave number was around $k=1.5$. In each plot,

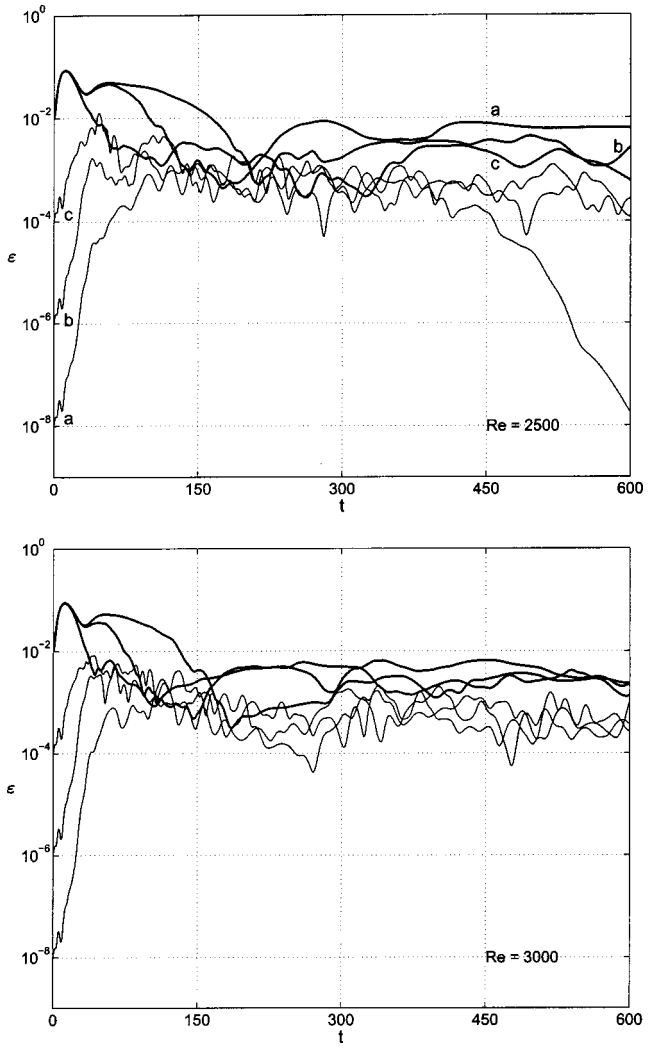

FIG. 4. Same as Fig. 3, for Re=2500, 3000.

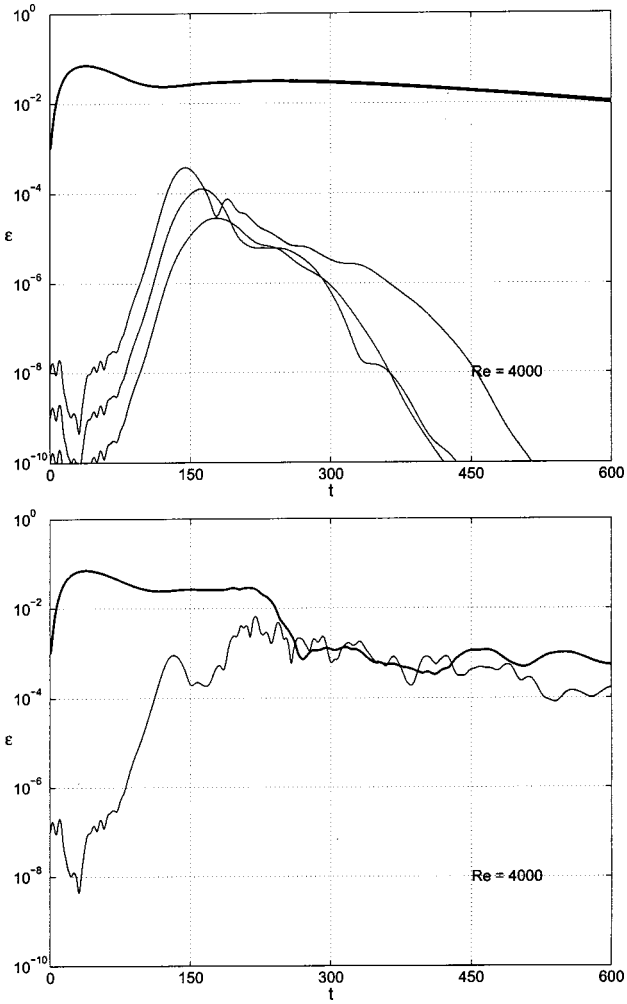

FIG. 5. Time evolution of the energy of 2D (thick curves) and 3D (thin curves) perturbations for Re=4000. At the top, the three-dimensional perturbations are too weak to destabilize the streak. At the bottom, a three-dimensional perturbation of energy 10^{-7} triggers instability. The spectral and time resolution in these computations was the same as in Figs. 3 and 4.

three independent integrations have been carried out, always starting with $\epsilon_0^{2D}=1\times10^{-2}$ and $\epsilon_0^{3D}=1\times10^{-4}$, $\epsilon_0^{3D}=1\times10^{-6}$ or $\epsilon_0^{3D}=1\times10^{-8}$. In this exploration, the spectral resolution was fixed to $M=14$ radial modes, $N=7$ azimuthal modes and $L=1$ axial modes, with a time step $\Delta t=5\times10^{-2}$. Many features should be pointed out. For Re=1000 (Fig. 3, top), the streaks do not appear, and the two and three dimensional energies decay almost monotonically for long times. We observe that the three-dimensional perturbations evolve almost identically in the three independent integrations. This is because the nonlinearities are still negligible at that stage and the evolution mechanism is basically linear. For Re=2000 (Fig. 3, bottom), the streaks already appear and we can identify for the first time the growth of the 3D-perturbation for the three cases, where we have labeled the three different evolutions in order to identify the energies corresponding to each one of the integrations. Nevertheless, this growth is only transient and the perturbations eventually decay. For Re=2500 (Fig. 4, top), only the smallest 3D-perturbation, for $\epsilon_0^{3D}=1\times10^{-8}$, is not strong enough to sustain the streak instability for $t>450$ (curve a), whereas the other two initial conditions clearly trigger transition (curves b and c), leading to a sustained chaotic evolution. Finally, for Re=3000 (Fig. 4, bottom), all the three-dimensional disturbances suffer an exponential instability, leading always to the streak breakdown phenomenon. In all the cases studied, the average lifetime of these turbulent or chaotic regimes depends drastically on the Reynolds number. Therefore, any small perturbation might eventually decay for t long enough, as observed for Re=2500 (Fig. 4, top), for $\epsilon_0^{3D}=1\times10^{-8}$. This would be in agreement with former numerical experiments where it was suggested that, even some perturbations may survive for long times, turbulence in this particular problem is only a transient phenomenon.[22]

In Fig. 5, we have carried out another computation for higher Reynolds number, Re=4000, and lower amplitude of the initial perturbation $\epsilon_0^{2D}=1\times10^{-3}$. This computation has been done in order to point out that the amplitude of the 3D-perturbation becomes crucial as long as the initial amplitude of the 2D-perturbation decreases. In the first case (top, Fig. 5), we see that three independent 3D-perturbations of energies $\epsilon_0^{3D}=1\times10^{-10,-9,-8}$, are not strong enough to destabilize the streak. We observe again the remarkable similarities of the evolution of the 3D-perturbations until they

reach their maximum amplification, where the linear mechanisms are much stronger than the nonlinear ones. In this case, the threshold three-dimensional energy for this instability mechanism is of order 10^{-7}; see Fig. 5, bottom. As mentioned before, the initial amplitude of the 2D-perturbation remarkably modifies the instability mechanism. This is reflected in the relative delay of the growth of the 3D-perturbations observed in Fig. 5 with respect to those seen in Figs. 3 and 4. For lower initial energies ϵ_0^{2D}, the streaks need longer times to appear and trigger growth of the 3D-modes. For example, for $\epsilon_0^{2D}=1\times10^{-2}$, the 3D-modes start growing almost exponentially for $t\gtrsim10$ approximately (Fig. 4). For $\epsilon_0^{2D}=1\times10^{-3}$ this growth does not start until $t\sim70$ (Fig. 5). The Reynolds number affects the slope of the exponential growth. When Re is increased from 2000 to 3000, the growth rate is increased as well (Fig. 3, bottom, and Fig. 4). This growth rate is also affected when the amplitude of ϵ_0^{2D} is decreased. Figure 5 shows that when the Reynolds number is increased to Re=4000, the growth rate of the 3D-modes is remarkably reduced.

In all previous computations, we only included one streamwise dependent mode, i.e., $L=1$. At a first glance, this may sound a bit drastic truncation and requires a numerical exploration to justify its validity. We have carried out computations including higher harmonics in the axial variable, that is increasing the spectral order L. The motivation for doing this is to check whether these higher frequencies substantially affect the streak breakdown mechanism or not. In Fig. 6, we have represented the time evolution of a same initial perturbation for increasing values of L for Re=4000 and $Q=\pi$. In these computations, we considered $N=7$ azimuthal modes, $M=14$ radial modes, $\Delta t=5\times10^{-2}$ and $L=1$, 3, 5 and 7. For all cases represented in Fig. 6, the initial condition is of the form given by Eq. (36), which originally assigns energy to the fundamental 3D-modes: $e^{\pm ikz}$, with $k=2$. The energies are distributed as before; $\epsilon_0^{3D}=1\times10^{-7}$ and $\epsilon_0^{2D}=1\times10^{-3}$. The higher harmonics $e^{\pm i2kz}$, $e^{\pm i3kz}$,..., might be activated afterward via nonlinear mechanisms and consequently affect the efficiency of the mechanism. Nevertheless, we can see that the four integrations lead to a streak breakdown and that the differences are not remarkable at all. Of course, the evolution is not identical (as expected), but the growth rate of the energy corresponding to the fundamental mode and the time at which the streak breakdown occurs is essentially the same in the four cases. We have proceeded knowing *a priori* that 3D-modes with axial wave numbers around $k\sim1.5$ were the most effective in this scenario [Zikanov, Ref. 15, Fig. 10(a)]. The nonlinear coupling would trigger higher frequencies which are away from that optimal value and it seems that they do not play a very relevant role in this transition.

So far, we have considered initial conditions where $\epsilon_0^{3D}\ll\epsilon_0^{2D}$, and this is key point of our study, i.e., providing more energy to the streamwise vortices in order trigger an inflexional instability potentially unstable with respect to very small 3D-modes. When $\epsilon_0^{3D}\sim\epsilon_0^{2D}$, increasing the number of axial modes does not remarkably affect the main features of the transition, but it may change the way energy is distributed once the breakdown has occurred. This phenomenon can be observed in Fig. 7, where we have plotted four evolutions of the same initial condition as before, initially feeding a fundamental streamwise-dependent mode and for increasing values of L. In this comparison we have considered the same values for M, N, L, and Δt as before, but with similar energies for the 2D and 3D perturbations; $\epsilon_0^{3D}=5\times10^{-4}$ and $\epsilon_0^{2D}=2\epsilon_0^{3D}$. In Fig. 7, we observe that the initial stages of the evolution of the 3D-mode is almost identical, with a very small transient growth at the beginning and a decreasing energy until the 2D-streaks are developed. After that, the 3D-modes start growing, eventually breaking the

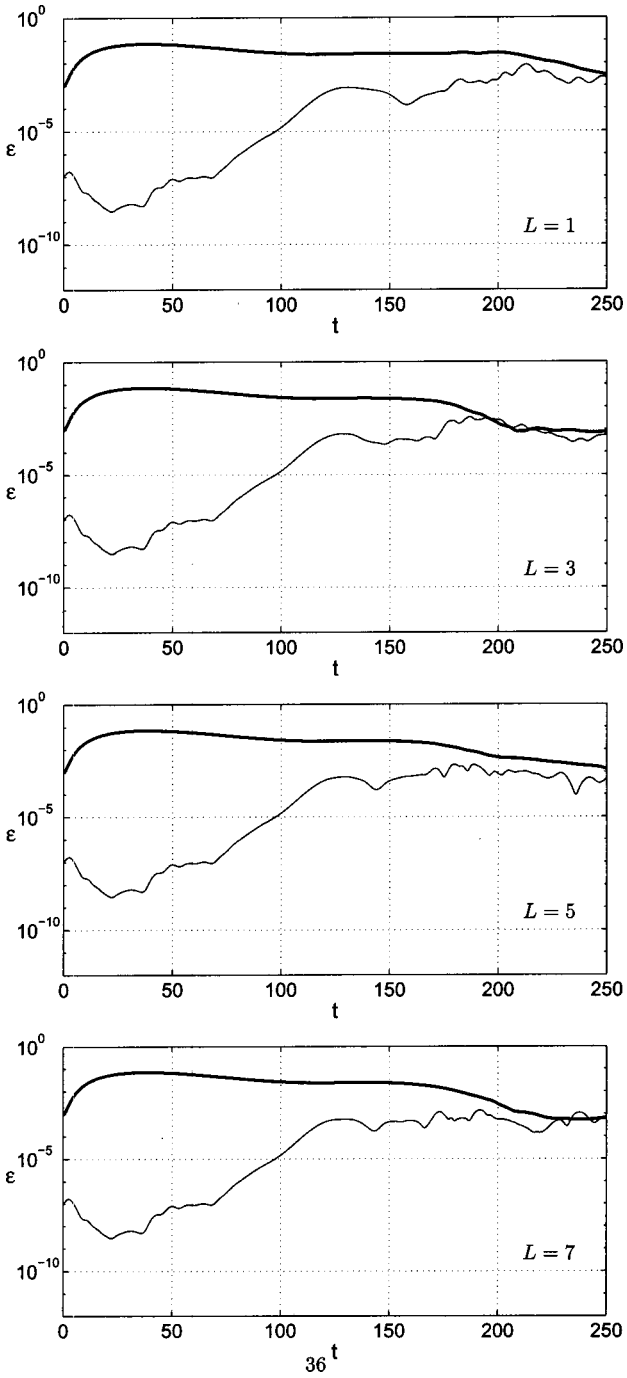

FIG. 6. Time evolution of a same initial perturbation for Re=4000 and different number of axial modes L.

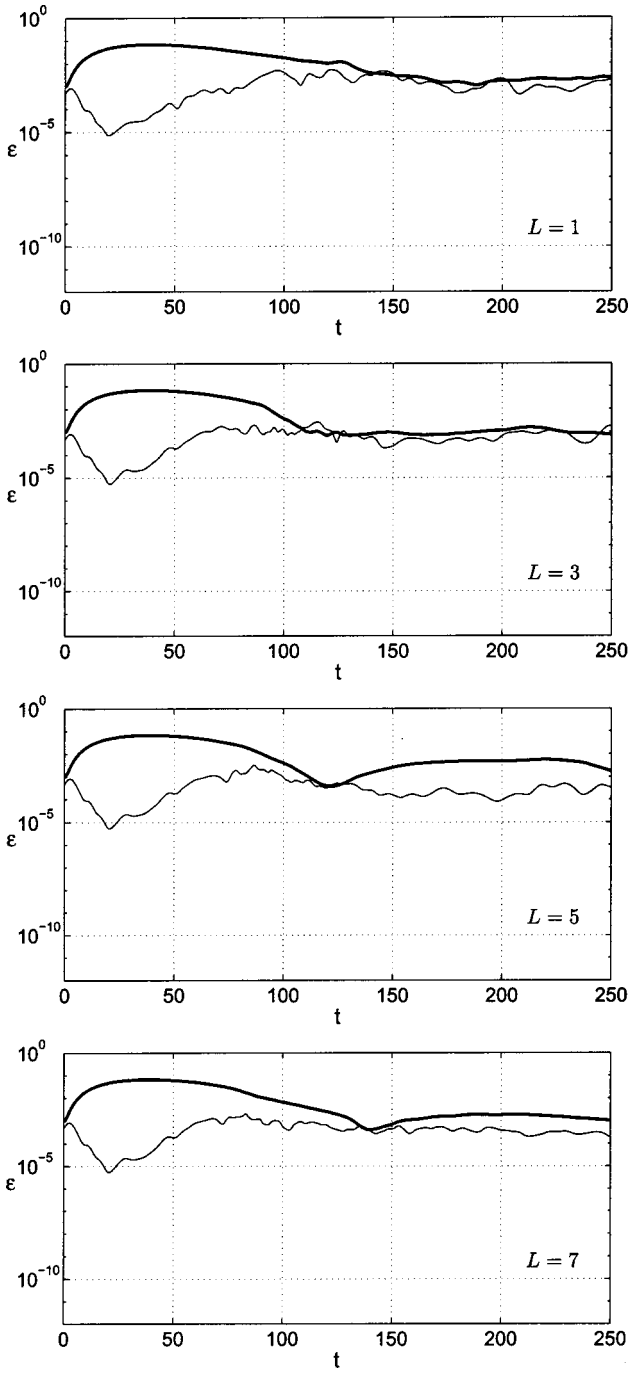

FIG. 7. Same as Fig. 6, but this time with similar initial energies for the 2D and 3D modes.

streaks for $t\in[100,150]$ in the four cases. After the streak breakdown has taken place, we observe a difference in the nonlinear evolution of the 3D and 2D modes. In particular, for $L=5$ and $L=7$, we observe what seems to be a refeeding of the 2D-streaks for $t\sim 200$, which appear again although weakener than before. This phenomenon seems to be similar to the *mother and daughter* scenario, originally suggested Boberg and Brosa,[4] where the 2D-modes (mothers) initially feed the 3D-modes (daughters), making them grow and instabilize the streaks. Once the mothers vanish, the daughters reconstruct them again, via nonlinear couplings, making the mothers reappear in order to repeat the cycle. This second instability is also known as *oblique transition*.[13]

V. THRESHOLD BOUNDARY OF TRANSITION

One of the main objectives in the study of subcritical transition in shear flows is to determine the topological features of the basin of attraction of the basic solution.[23] Since the minimum amplitude required to destabilize the flow decreases when increasing the Reynolds number, it is clear that the size of this manifold must necessarily shrink as well. In a recent asymptotic analysis provided by Chapman[24] for plane channel flows, it has been proved that the threshold amplitude required for transition decreases with the Reynolds number like $A_c\sim \mathrm{Re}^{\gamma}$, where $\gamma=-5/4$ for plane Poiseuille flow and $\gamma=-1$ for plane Couette. Of course, the previous threshold exponents are only meaningful in the context of asymptotic ranges of the Reynolds number. For intermediate and even moderately high Reynolds numbers, the critical amplitude has to be computed either numerically or experimentally. A first attempt at reconciliation regarding the value of γ obtained in laboratory experiments and numerical simulations has been recently provided by Trefethen *et al.*[25] Two main problems arise when trying to compare theoretical asymptotics with numerical and experimental results. First, asymptotic results are impossible to produce in the laboratory due to the fact that the pipe has a finite length. Since the streaks appear after a period of time of order $O(\mathrm{Re})$,[24] this would require very long pipes in order to observe the eventual transition. Second, from a numerical point of view, it is very difficult to provide comparable simulations reproducing the real initial conditions for the experimental perturbations. In the experiments, fluid is injected from the pipe wall, violating the assumption of homogeneous boundary condition for the perturbation field (13). Our main purpose has been to include a coarse three-dimensionality in the nonlinear initial value problem in order to explore the streak breakdown mechanism based on different initial amplitudes of the perturbation field and values of the Reynolds number.

In order to make a consistent computation based on the experimental time specifications, we considered time integrations in the interval $0\leqslant t\leqslant T=250$, i.e., the time required by a fluid particle located at the pipe axis to be advected downstream by the basic Hagen–Poiseuille flow a distance of 125 pipe diameters. According to the experiments of Darbyshire and Mullin, henceforth referred as D&M, the perturbation was injected 70 pipe diameters downstream of the pipe inlet and 120 upstream from the outlet. Even the mechanisms of transition presented here may slightly differ from the ones triggered in the experiments, each one of our numerical runs should cover the transition dynamics observed in the laboratory. We considered the same perturbations as the ones used in the previous sections, always starting with $\boldsymbol{\epsilon}_0^{3\mathrm{D}}=1\times10^{-7}$ and $\boldsymbol{\epsilon}_0^{2\mathrm{D}}$ ranging from 9×10^{-6} to 2×10^{-2}. We included only one streamwise-dependent mode in the integration of axial wave number $k=2\pi/Q=1.5$ which is a good candidate to trigger transition according to Zikanov's linear computations. Our criteria of identification of sustained chaotic evolution was based on the energy of the 3D-

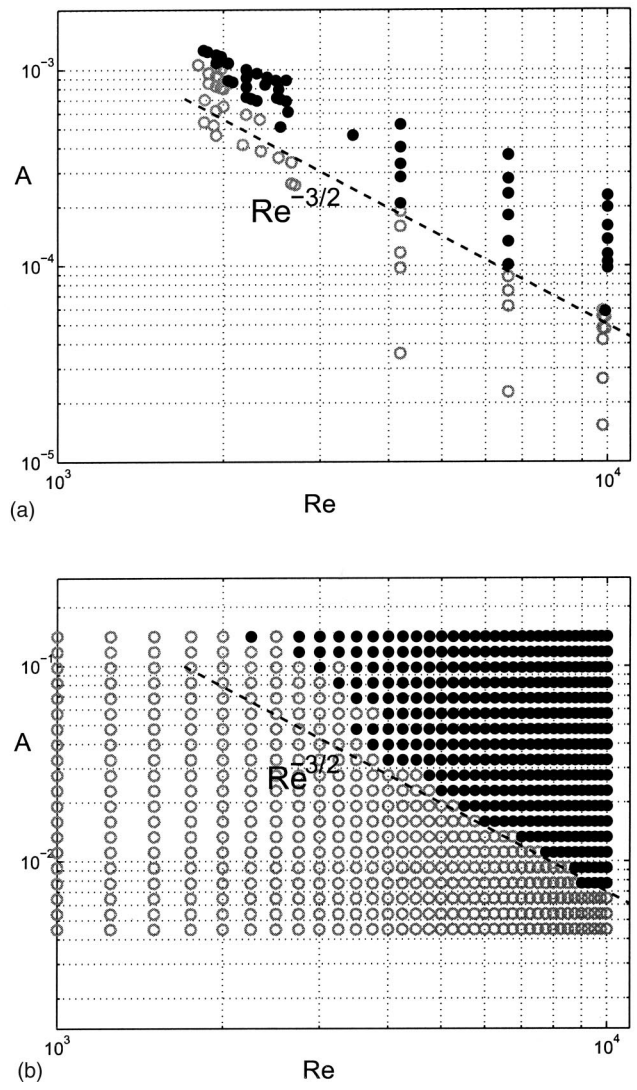

FIG. 8. Experimental analysis provided by Darbyshire and Mullin (Ref. 3) (top, a) and numerical results (bottom, b). In both plots, black dots represent those situations were the flow became turbulent, whereas white dots represent relaminarization.

perturbation at the end of each run. In particular, we classified the run as successful if $\boldsymbol{\epsilon}^{3D}(t=T)>1\times10^{-4}$, i.e., at the end of the run, the energy associated with the 3D-perturbation was still three orders of magnitude bigger than its initial value. For the exploration, the spectral resolution was fixed to $N=5$ azimuthal modes, $M=14$ radial solenoidal modes and $L=1$ axial modes, and the time step was $\Delta t=5\times10^{-2}$. No qualitative differences were found when increasing the number of spectral modes or reducing the time step. Overall, the number of degrees of freedom in the integrated system (26) was 1350.

We carried out 740 runs whose final results have been outlined an compared with the experimental results in Fig. 8. According to a recent comparative analysis between experiments and numerics,[25] the critical amplitudes reported by D&M[3] were measured in different units from the theoretical and numerical results. To make a consistent comparison it is necessary to divide the D&M results by one power of Re, giving $\gamma\sim-3/2$, and this has been done in Fig. 8(a). Thus Fig. 8(a) represents not the original plot from D&M[3,25] but a reprocessing of that data to make a comparison [the numbers on the vertical scale of Fig. 8(a) are subject to an arbitrary constant; thus the discrepancy of the vertical axes labels on the figure is not significant]. In Fig. 8(a), black dots represent experimental transition to turbulence and white dots represent relaminarization of the flow within the pipe domain. In Fig. 8(b), we have represented the numerical results of our integrations. The amplitude A on the ordinate axis represents the square root of the total initial energy of the perturbation given by

$$A=\sqrt{\boldsymbol{\epsilon}_0^{3D}+\boldsymbol{\epsilon}_0^{2D}}. \tag{40}$$

White dots represent those situations where the flow relaminarized by the time the run was ended. Black dots represent successful transition. Despite the coarse numerical approximation of the problem, we observe a significant agreement with the experimental observations. First, according to our computations [Fig. 8(b)], there is no transition for Re$\lesssim$2000. Second, the threshold amplitude decreases in both cases quite similarly. We have included a straight line in both plots representing the asymptotic curve $\mathrm{Re}^{-3/2}$ in order to compare the experimental and numerical behavior. As we see, the agreement is very good. Nevertheless, it is probably too early to associate this apparent agreement with a common mechanism of transition. In both explorations, the Reynolds number is far from being within an asymptotic range. In fact, the analyses have been done still very close to the vertical threshold (Re$\sim$2000), thus strongly affecting the slope of the threshold boundary. To put it mildly, experiments and numerics are both providing the same *local* slope, none of them being asymptotic. Besides, in our computations, the perturbations were global, and periodic, whereas in the experiments the flow was perturbed locally thus triggering very high axial and azimuthal modes from the beginning. At a first glance, we could argue that the nonlinear selection rules, in combination with the nonnormal linear operator acting on the experimental perturbation could lead to a specific selection of streamwise-independent structures which eventually are responsible for the transition. We have not explored other more complicated scenarios such as *oblique transition*,[14,24] which has been proved to be slightly more efficient in plane channel flows. In any case, the author *does not* claim that the streak breakdown is the only responsible for that transition by itself. Certainly, the mechanism explored here provides a consistent explanation if we compare with the experiments, but the real dynamics occurring in the laboratory are far from being understood.

VI. CONCLUSIONS

A comprehensive exploration of the streak breakdown instability mechanism for pipe flow has been provided. The analysis has been based on the numerical integration of the nonlinear Navier–Stokes equations for the perturbation fields. We have considered specific initial perturbations based on linear stability analyses of time-dependent modulated flows provided by other authors. In particular, we used very small streamwise-dependent disturbances that, added to

the finite amplitude streamwise-independent perturbation, undergone an optimal growth in the time-dependent linear stability analysis carried out in previous works. In all cases studied, the agreement with the experimental results is very good, shedding some light on the internal mechanisms responsible for transition in these type of flows. The oblique transition of spiral modes may also be at work in the experiments. This will be explained in a future study.

ACKNOWLEDGMENTS

This work was supported by the UK EPSRC under Grant No. GR/M30890. The author thanks Nick Trefethen for fruitful discussions.

APPENDIX: SOLENOIDAL BASES

In what follows, we define

$$h_m(r)=(1-r^2)T_{2m}(r),\quad g_m(r)=(1-r^2)h_m(r),\qquad D=\frac{d}{dr},\quad D_+=D+\frac{1}{r},\tag{A1}$$

where T_{2m} is the Chebyshev polynomial of degree $2m$ and $r\in(0,1)$. The $1-r^2$ factors are included in order to inforce homogeneous boundary conditions at the pipe wall. We begin with the *trial* functions $\mathbf{\Phi}_{lnm}(r,\theta,z)$, distinguishing two cases depending on whether n is zero or nonzero.

Case $n=0$. The basis is spanned by the elements

$$\mathbf{\Phi}^{(1)}_{l0m}=e^{i(2\pi/Q)lz}\mathbf{v}^{(1)}_{l0m}=e^{i(2\pi/Q)lz}\begin{pmatrix}0\\ rh_m(r)\\ 0\end{pmatrix},\tag{A2}$$

$$\mathbf{\Phi}^{(2)}_{l0m}=e^{i(2\pi/Q)lz}\mathbf{v}^{(2)}_{l0m}=e^{i(2\pi/Q)lz}\begin{pmatrix}-\dfrac{2\pi}{Q}ilrg_m(r)\\ 0\\ D_+[rg_m(r)]\end{pmatrix},\tag{A3}$$

except that if $l=0$, the third component of $\mathbf{\Phi}^{(2)}_{lnm}$ is replaced by $h_m(r)$.

Case $n\neq 0$. In this case, the basis is spanned by the elements

$$\mathbf{\Phi}^{(1)}_{lnm}=e^{i(n\theta+(2\pi/Q)lz)}\mathbf{v}^{(1)}_{lnm}=e^{i(n\theta+(2\pi/Q)lz)}\begin{pmatrix}-inr^{\sigma-1}g_m(r)\\ D[r^{\sigma}g_m(r)]\\ 0\end{pmatrix},\tag{A4}$$

$$\mathbf{\Phi}^{(2)}_{lnm}=e^{i(n\theta+(2\pi/Q)lz)}\mathbf{v}^{(2)}_{lnm}=e^{i(n\theta+(2\pi/Q)lz)}\begin{pmatrix}0\\ -i\dfrac{2\pi}{Q}lr^{\sigma+1}h_m(r)\\ inr^{\sigma}h_m(r)\end{pmatrix},\tag{A5}$$

where, following the regularization rules proposed in Ref. 7, $\sigma=2$ for n even and $\sigma=1$ for n odd.

For the *test* functions $\mathbf{\Psi}_{lnm}(r,\theta,z)$, we could take the same basis. However, the resulting matrices appearing in Eqs. (27) and (28) would be dense, whereas they can be made to be banded if one chooses the projection bases as follows:

Case $n=0$.

$$\mathbf{\Psi}^{(1)}_{l0m}=e^{i(2\pi/Q)lz}\tilde{\mathbf{v}}^{(1)}_{l0m}(r)=e^{i(2\pi/Q)lz}\begin{pmatrix}0\\ h_m(r)\\ 0\end{pmatrix}\frac{1}{\sqrt{1-r^2}},$$
$$\mathbf{\Psi}^{(2)}_{l0m}=e^{i(2\pi/Q)lz}\tilde{\mathbf{v}}^{(2)}_{l0m}(r)=e^{i(2\pi/Q)lz}\begin{pmatrix}-\dfrac{2\pi}{Q}ilr^2g_m(r)\\ 0\\ D_+[r^2g_m(r)]+r^3h_m(r)\end{pmatrix}\frac{1}{\sqrt{1-r^2}},\tag{A6}$$

except that the third component of the vector in $\mathbf{\Psi}^{(2)}_{l0m}$ is replaced by $rh_m(r)$ if $l=0$.

Case $n\neq 0$.

$$\mathbf{\Psi}^{(1)}_{lnm}=e^{i(n\theta+(2\pi/Q)lz)}\tilde{\mathbf{v}}^{(1)}_{lnm}(r)=e^{i(n\theta+(2\pi/Q)lz)}\begin{pmatrix}inr^{\beta}g_m(r)\\ D[r^{\beta+1}g_m(r)]+r^{\beta+2}h_m(r)\\ 0\end{pmatrix}\frac{1}{\sqrt{1-r^2}},$$
$$\mathbf{\Psi}^{(2)}_{lnm}=e^{i(n\theta+(2\pi/Q)lz)}\tilde{\mathbf{v}}^{(2)}_{lnm}(r)=e^{i(n\theta+(2\pi/Q)lz)}\begin{pmatrix}0\\ -\dfrac{2\pi}{Q}ilr^{\beta+2}h_m(r)\\ inr^{\beta+1}h_m(r)\end{pmatrix}\frac{1}{\sqrt{1-r^2}},\tag{A7}$$

except that the third component of the vector in $\mathbf{\Psi}^{(2)}_{lnm}$ is replaced by $r^{1-\beta}h_m(r)$ if $l=0$, where $\beta=0$ for n even and $\beta=1$ for n odd. These vector fields include the Chebyshev factor $(1-r^2)^{-1/2}$ so that the products between the test and trial functions can be exactly calculated via Gauss–Lobatto quadrature, leading to banded matrices. We note that the radial variable runs from 0 to 1, and not from -1 to 1, as would expected by using Chebyshev polynomials. This inforces the appropiate symmetry and regularity conditions on the axis.

[1] P. G. Drazin and W. H. Reid, *Hydrodynamic Stability* (Cambridge University Press, Cambridge, 1981).
[2] I. J. Wygnanski and F. H. Champagne, "On transition in a pipe. Part I. The origin of puffs and slugs and the flow in a turbulent slug," J. Fluid Mech. **59**, 281 (1973).
[3] A. G. Darbyshire and T. Mullin, "Transition to turbulence in constant-mass-flux pipe flow," J. Fluid Mech. **289**, 83 (1995).
[4] L. Boberg and U. Brosa, "Onset of turbulence in a pipe," Z. Naturforsch., A: Phys. Sci. **43**, 697 (1988).
[5] A. Leonard and W. Reynolds, "Turbulent research by numerical simulation," in *Perspectives in Fluid Mechanics*, edited by D. Coles (Springer-Verlag, New York, 1988), pp. 113–142.
[6] P. L. O'Sullivan and K. S. Breuer, "Transient growth in circular pipe flow. II. Nonlinear development," Phys. Fluids **6**, 3652 (1994).
[7] V. G. Priymak and T. Miyazaki, "Accurate Navier–Stokes investigation of transitional and turbulent flows in a circular pipe," J. Comput. Phys. **142**, 370 (1998).

[8]H. Shan, B. Ma, Z. Zhang, and F. T. M. Nieuwstadt, ''Direct numerical simulation of a puff and slug in transitional cylindrical pipe flow,'' J. Fluid Mech. **389**, 39 (1999).
[9]J. Komminaho, ''Direct numerical simulation of turbulent flow in plane and cylindrical geometries,'' Doctoral Thesis, Royal Institute of Technology, Stockholm (2000).
[10]P. J. Schmid and D. S. Henningson, ''Optimal energy growth in Hagen–Poiseuille flow,'' J. Fluid Mech. **277**, 197 (1994).
[11]A. Meseguer and L. N. Trefethen, ''A spectral Petrov–Galerkin formulation for pipe flow I: Linear stability and transient growth,'' Oxford University, Numerical Analysis Group, Report 00/18 (2000).
[12]C. R. Reddy and D. S. Henningson, ''On the role of linear mechanisms in transition to turbulence,'' Phys. Fluids **6**, 1396 (1994).
[13]P. J. Schmid and D. S. Henningson, *Stability and Transition in Shear Flows* (Springer-Verlag, New York, 2001).
[14]S. C. Reddy, P. J. Schmid, J. S. Baggett, and D. S. Henningson, ''On stability of streamwise streaks and transition thresholds in plane channel flows,'' J. Fluid Mech. **365**, 269 (1998).
[15]O. Y. Zikanov, ''On the instability of pipe Poiseuille flow,'' Phys. Fluids **8**, 2923 (1996).
[16]G. K. Batchelor, *An Introduction to Fluid Dynamics* (Cambridge University Press, Cambridge, 1967).
[17]C. Canuto, M. Y. Hussaini, A. Quarteroni, and T. A. Zang, *Spectral Methods in Fluid Dynamics* (Springer-Verlag, New York, 1988).
[18]A. Leonard and A. Wray, ''A new numerical method for the simulation of three dimensional flow in a pipe,'' *Proceedings of the 8th International Conference on Numerical Methods in Fluid Dynamics*, edited by E. Krause (Springer-Verlag, Berlin, 1982).
[19]S. M. Cox and P. C. Matthews, ''Exponential time differencing for stiff systems,'' J. Comput. Phys. **176**, 430 (2001).
[20]E. Hairer and G. Wanner, *Solving Ordinary Differential Equations II: Stiff and Differential-Algebraic Problems* (Springer-Verlag, Berlin, 1991).
[21]M. T. Landahl, ''A note on an algebraic instability of inviscid parallel shear flows,'' J. Fluid Mech. **98**, 243 (1980).
[22]U. Brosa, ''Turbulence without strange attractor,'' J. Stat. Phys. **55**, 1303 (1989).
[23]B. Eckhardt and A. Mersmann, ''Transition to turbulence in a shear flow,'' Phys. Rev. E **60**, 509 (1999).
[24]S. J. Chapman, ''Subcritical transition in channel flows,'' J. Fluid Mech. **451**, 35 (2002).
[25]L. N. Trefethen, S. J. Chapman, D. S. Henningson, A. Meseguer, T. Mullin, and F. T. M. Nieuwstadt, ''Threshold amplitudes for transition to turbulence in a pipe,'' Numer. Anal. Rep. 00/17, Oxford University Comp. Lab. (2000).